IFSCC 2025 full paper (IFSCC2025-1458)

Resveratrol-Laden Tocofersolan Nanomicelles as A New Generation Anti-Photoaging Formulation for *In Situ* Transdermal Administration

LOUIS CHEW YU JIN *; FAN TANG
Guangdong Aili Biotechnology Co., Ltd, Guangzhou, P. R. China.

Abstract
Resveratrol, a natural polyphenol with a resorcinol and benzene-ethylene-benzene conjugated structure, holds significant potential for anti-aging applications due to its potent antioxidant and anti-inflammatory properties. However, prolonged exposure to air can lead to resveratrol oxidation, and it is also challenging for resveratrol to effectively penetrate the epidermis and exert its anti-melanogenesis effects. To address these challenges, tocofersolan was used to encapsulate resveratrol, forming nanomicelles (R@T-NM) with enhanced stability and transdermal delivery ability. The amphiphilic structure and inherent antioxidant properties of tocopherol provide spatial and molecular protection for resveratrol. In vitro experimental results demonstrate that R@T-NM, as a novel in situ transdermal drug delivery system, can significantly enhance the transdermal b ioavailability, antioxidant efficacy, and anti-aging effects of resveratrol. The developed R@T-NM system represents an innovative transdermal delivery platform, providing novel insights and methodologies for developing anti-photoaging therapeutics.

Keywords
Resveratrol, Tocofersolan, Antioxidant, Anti-photoaging, Anti-melanogenesis

---

1. Introduction

Ultraviolet (UV) radiation is an unavoidable environmental factor in daily life [1]. While moderate UV exposure facilitates calcium synthesis in the body, excessive UV exposure can induce various skin disorders and even carcinogenesis [2]. Skin photoaging is a progressive damage process caused by chronic UV irradiation, characterized by oxidative stress, inflammatory responses, and collagen degradation, ultimately leading to wrinkles, hyperpigmentation, and impaired skin barrier function [3]. With growing public awareness of skin health and aesthetics, the development of effective anti-photoaging agents has become a major research focus [4].

In recent years, natural polyphenolic compounds have received significant attention in the field of anti-photoaging due to their remarkable antioxidant and anti-inflammatory properties [5]. Among these, resveratrol (RES), a bioactive natural compound featuring a resorcinol and benzene-ethylene-benzene conjugated structure (**Scheme 1**), exhibits potent free radical scavenging capacity [6]. This enables effective suppression of reactive oxygen species (ROS)-mediated cellular damage, thereby delaying skin aging processes [7]. Furthermore, resveratrol

demonstrates substantial protective effects against UV-induced photoaging, oxidative damage, and hyperpigmentation through multiple mechanisms, including modulation of the NRF2 signaling pathway [8], inhibition of melanogenic enzyme activity [9], and suppression of the inflammatory response [10]. However, the practical application of resveratrol faces two critical challenges [11]. First, its inherent photosensitivity and susceptibility to oxidation compromise stability. Second, its low water-solubility significantly limits bioavailability and transdermal absorption efficiency. To address these limitations, researchers have investigated various drug delivery systems. Among them, polymeric nanomicelles have emerged as a particularly promising solution due to their unique structural characteristics and functional advantage [12].

Polymersome nanomicelles are self-assembled colloidal nanoparticles formed by amphiphilic molecules, featuring a distinctive core-shell architecture with hydrophilic coronas and hydrophobic cores [13]. This unique structural organization enables efficient encapsulation of hydrophobic drugs while significantly enhancing their stability and aqueous solubility [14]. Tocofersolan (D-α-tocopheryl polyethylene glycol succinate, TPGS), a widely used nanomicellar carrier material, exhibits excellent biocompatibility and superior self-assembling ability [15]. In this study, we developed resveratrol-laden TPGS nanomicelles (R@T-NM) via self-assembly technology, which demonstrate enhanced stability and remarkable transdermal delivery ability [16]. This nano-delivery system not only significantly enhances resveratrol stability by preventing its possible oxidative degradation but also improves cutaneous retention and absorption through the combined advantages of micellar nanostructure (particle size < 20 nm) and the permeation-enhancing properties of TPGS. More importantly, resveratrol and TPGS exhibit synergistic effects, demonstrating superior ROS scavenging capacity, anti-inflammatory activity, photoprotective efficacy, and melanogenesis inhibition ability compared to resveratrol alone.

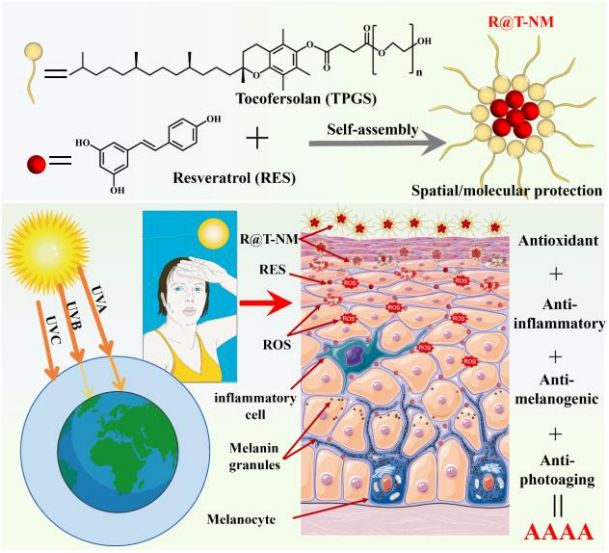

Scheme 1. Development of resveratrol-laden tocofersolan nanomicelles (R@T-NM) via self-assembly as a new generation antioxidant, anti-inflammatory, anti-melanogenic, and anti-photoaging (AAAA) formulation for in situ transdermal administration**.**

2. Methods and Characterizations.

2.1. Materials

Resveratrol, dipropylene glycol，glabridin (GL) and lipopolysaccharide (LPS) were purchased from Shanghai Macklin Biochemical Technology Co., Ltd (Shanghai, China). Fluorescein isothiocyanate (FITC) labeled resveratrol (FITC-RES) was from Xingbeiaike biotechnology Co., Ltd (Shanxi, China). Reactive oxygen species assay kit was purchased from Beyotime Biotechnology (Shanghai, China). Human interleukin 6 (IL-6) and human interleukin 8 (IL-8) ELISA

Kits were purchased from Bioswamp Life Science Lab (Wuhan, China), tyrosinase activity assay kit, senescence-associated β-galactosidase (SA-β-Gal) staining kit and tocofersolan were purchased from Solarbio technology Co., Ltd (Beijing, China).

2.2. Synthesis of R@T-NM

Resveratrol (1.5 wt%) was dissolved in dipropylene glycol by heating the mixture to 90°C until a homogeneous solution (Solution A) was obtained. Then TPGS (7.5 wt%) was added to Solution A, and the mixture was stirred at 90°C until a uniform dispersion (Solution B) was formed. Solution B was slowly added to deionized water to form a solution with TPGS concentration of 1 mg/mL. The temperature was maintained at 50-70 °C throughout the process, and continuous stirring was applied to ensure uniform dispersion, resulting in the formation of R@T-NM micelles. Glabridin-laden TPGS nanomicelles (G@T-NM) were prepared in the same way.

2.3. Characterizations of R@T-NM

Stability Testing: The R@T-NM was stored at room temperature and the appearance change were observed and photographed after one week. Meanwhile, the homogeneity of the R@T-NM solution was examined by irradiating it with a laser pointer to evaluate the formulation stability.

Morphological Observation: The R@T-NM system was diluted with water to an appropriate concentration and then drop-cast onto a copper grid. After air-drying the copper grid at room temperature, the morphology of R@T-NM was examined using transmission electron microscopy (TEM, FEI TecnaiG2 20 S-Twin).

Measurement of Particle Size and Zeta Potential: The R@T-NM sample was diluted to 1 mg/mL, then charged into a polystyrene (PS) sizing cuvette or a U-shaped capillary cell (DTS0012). Particle sizes and zeta potentials were determined by dynamic light scattering (DLS). Three independent replicates were performed for each group and the results were averaged.

2.4 Validation of transdermal effect of R@T-NM in 3D Cellular Skin Models

Methacryloyl gelatin (GelMA, 15 wt%, 100 μL) supplemented with lithium phenyl-2,4,6-trimethylbenzoylphosphinate (LAP) photoinitiator (0.1 wt%) was added into a Transwell chamber and crosslinked under UA light to form a hydrogel. An adequate number of cells were seeded atop the hydrogel to create a cellular layer to mimic the 3D structure of skin with a dense epidermis and relatively loose subcutaneous tissue. After 24-hour incubation in a 24-well plate, the culture medium was removed, and an FITC-R@T-NM (FITC-Res laden in TPGS nanomicelles) solution (1 wt%) was added to the upper chamber with the created 3D cellular skin model. After incubating for 24 hours, the hydrogel was examined by fluorescence microscopy to evaluate the transmission of FITC-R@T-NM in the 3D cellular skin model.

2.5 Biocompatibility of R@T-NM

Human skin fibroblasts (HSF) were cultured in complete DMEM supplemented with 10% (v/v) fetal bovine serum (FBS) and 1% (v/v) penicillin/streptomycin in a humidified incubator (Thermo Fisher Scientific, USA) at 37°C with 5% CO_2. The cytotoxicity of R@T-NM against HSF was assessed using CCK-8 assay and Live/Dead staining kit. R@T-NM with various concentrations was prepared in PBS and sterilized by filtration through a 0.2 μm membrane. HSF were seeded in 96-well plates at a density of 4 × 10^4 cells/mL and 200 μL/well and cultured under optimal conditions overnight to allow attachment. Cells were then treated with complete medium containing different concentrations of R@T-NM for 24 hours. After removing the medium, the configured CCK-8 reaction solution was added to each well and incubated for another 2 hours in incubator. Optical density (OD) was quantified by measuring absorbance at 450 nm. Cells cultured in complete DMEM was served as the control group. Cell viability was

calculated using the following equation: Cell viability (%) = (A_b - A_s) / (A_c - A_s) × 100%, where A_b represents the absorbance of test samples at 450 nm, A_c represents the absorbance of the control sample at 450 nm, and A_s is the OD value of CCK-8 reaction solution.

Additionally, cells were labeled with a Live/Dead staining kit (AO/EB Staining Kit and observed under an inverted fluorescence microscope (IX53, Olympus). Each group was tested in triplicate.

2.6 Assessment of the antioxidant effect

DPPH Radical Scavenging Assay: R@T-NM at a concentration of 1 mg/mL was added to a 0.12 mg/mL DPPH ethanol solution. After incubating in the dark for a predetermined period, the absorbance of the treated DPPH solution was measured at 517 nm (A_s) using a UV-Vis spectrophotometer. The absorbance of the untreated DPPH solution (A_b) was used as the blank control. The DPPH scavenging rate was calculated using the following equation: DPPH scavenging rate (%) = (A_b−A_s)/ A_b ×100%.

Intracellular ROS Scavenging Assay: HSF cells were seeded in 24-well plates and cultured until reaching 80-90% confluence. Then HSF cells were pretreated with hydrogen peroxide (H_2O_2) for 30 minutes, followed by incubation with R@T-NM-containing medium (10 μg/mL) for 24 hours. After treatment, the R@T-NM-containing medium was removed, and the cells were washed with PBS. DCFH-DA was diluted 1:1000 in serum-free medium, and 1 mL of the configured DCFH-DA reaction solution was added to each well. Cells were incubated with DCFH-DA in the dark for 30 minutes at 37°C. Then the DCFH-DA solution was aspirated and cells were washed three times with serum-free medium to remove residual probe. Fluorescence images were acquired using an inverted fluorescence microscope, and fluorescence intensity was quantified using ImageJ software.

2.7 Detection of Inflammatory Cytokine Expression

HSF cells were seeded in 24-well plates and cultured until reaching 80-90% confluence. Cells were then pretreated with the inflammatory stimulant LPS, followed by incubation with R@T-NM-containing complete DMEM for 24 hours. After treatment, cell culture supernatants were collected and analyzed for IL-6 and IL-8 levels using commercial ELISA kits according to the manufacturer's protocol. Absorbance (OD values) was measured at 450 nm using a microplate reader, and cytokine concentrations were calculated based on standard curves.

2.8 Cellular photoaging assay

HSF cells and fibroblasts were seeded in 24-well or 12-well plates and cultured to 50-60% confluence. HSF cells were covered with PBS and exposed to UVA irradiation at a total dose of 5 J/cm² per session. Following irradiation, PBS was removed and replaced with R@T-NM-containing complete DMEM. This irradiation protocol was repeated daily for 5 consecutive days. For senescence assessment, cells in 24-well plates were stained using a senescence-associated β-galactosidase (SA-β-gal) staining kit according to the manufacturer's instructions. Concurrently, cellular NAD^+ content in 12-well plates was quantified using a commercial NAD^+ detection kit according to the manufacturer's instructions.

2.9 Anti-melanogenesis activity assay

The melanoma cells were seeded in 12-well plates and cultured until reaching 80-90% confluence. Cells were then treated with R@T-NM-containing complete DMEM for 72 h. Intracellular tyrosinase activity was measured using a commercial tyrosinase activity assay kit according to the manufacturer's protocol.

2.10 Statistical analysis

All the experimental data were statistically analyzed and expressed as mean ± standard deviation (SD), and the statistical difference was determined by t-test or one-way ANOVA. All the data are considered to have significant differences only when $p < 0.05$. * and ** represent $p < 0.05$ and $p < 0.01$, respectively.

3. Results.

3.1. Characterizations of R@T-NM

As shown in **Figure 1A**, the encapsulation of resveratrol in TPGS resulted in a transparent and clear R@T-NM solution, whereas the unencapsulated resveratrol solution appeared turbid with substantial flocculent precipitates suspended in the solution. The Tyndall effect was observed when the prepared R@T-NM was irradiated with a laser beam, confirming the formation of a colloidal sol system rather than a true molecular solution. Furthermore, the R@T-NM formulation maintained excellent physical stability after 7 days of storage at 37°C, with no visible phase separation or drug precipitation, demonstrating its robust stability.

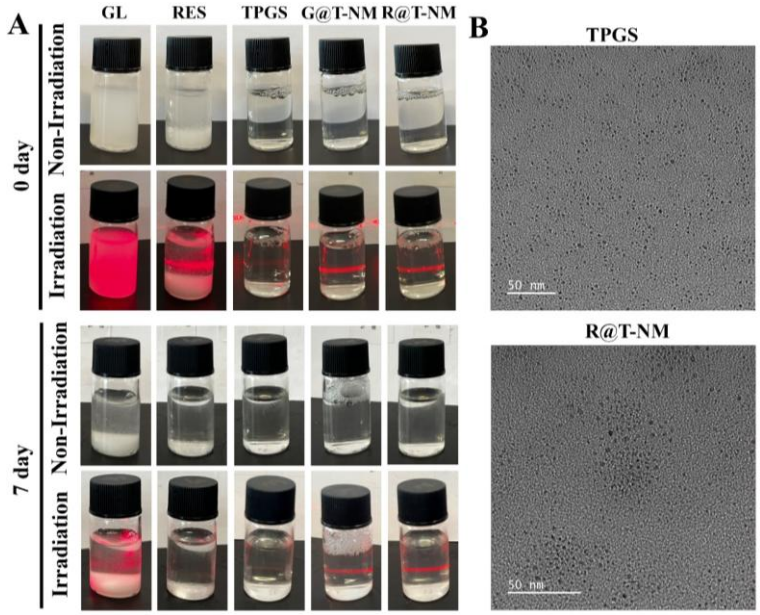

Figure 1. A) Stability test images and the Tyndall effect of R@T-NM. B) TEM images of R@T-NM.

As shown in **Figure 1B**, TEM revealed that R@T-NM nanoparticles exhibited a transparent, uniform, and spherical morphology. Dynamic light scattering (DLS) analysis demonstrated an average particle size of 16.52 nm with a zeta potential of -2.473 mV, indicating a negatively charged surface. This negative surface charge promotes electrostatic repulsion between R@T-NM nanoparticles, thereby enhancing their dispersibility and contributing to the system's stability. To further support this observation, the polydispersity index (PDI) values of resveratrol (RES; 0.7033) and TPGS (0.5182) were significantly higher than that of R@T-NM (0.09319) (**Table 1**), confirming the superior homogeneity of molecular distribution within the R@T-NM system. Comparative zeta potential analysis revealed that R@T-NM exhibited significantly higher surface charge (-2.47 mV) compared to unformulated resveratrol (RES) (-49.98 mV) and TPGS alone (-13.07 mV), indicating markedly reduced reducibility of the encapsulated RES. The enhanced stability might be arises through two synergistic mechanisms: (1) electronic modulation via TPGS-mediated alteration of RES's electron density distribution through potential covalent bonding or non-covalent interactions (e.g., hydrogen bonding and π-π stacking), which stabilizes the phenolic redox centers [17]; and (2) spatial protection whereby the

TPGS matrix physically shields RES's reactive hydroxyl groups through three-dimensional encapsulation, thereby limiting accessibility to free radicals and oxidative species. These dual stabilization pathways collectively contribute to the improved antioxidant performance and chemical stability observed in the R@T-NM formulation [18].

Table 1. Particle Size and Zeta Potential R@T-NM

	RES	TPGS	R@T-NM
Z-Average (nm)	9711.67 ± 1737.09	21.61 ± 0.80	16.52 ± 0.02
Zeta Potential (mV)	-49.98 ± 33.88	-13.07 ± 5.44	-2.47 ± 1.30
Polydispersity Index (PI)	0.70 ± 0.20	0.51 ± 0.028	0.09 ± 0.008

3.2. Validation of Transdermal Permeation Using 3D Cellular Skin Model

For drug permeation studies, human skin represents the ideal penetration barrier [19]. However, ethical constraints limit the availability of natural human skin, while the reliability of artificially cultured human skin remains under evaluation and its high cost prohibits large-scale acquisition. Therefore, we employed a GelMA-based cellular scaffold to simulate the extracellular matrix in vitro. As demonstrated in Figure 2A, the GelMA hydrogel exhibited a bilayer structure: an upper dense porous layer corresponding to the epidermal stratum and a lower relatively loose porous layer mimicking the dermal stratum, collectively forming a skin-like barrier. Notably, the hydrogel surface showed substantial cell attachment (Figure 2B). Following application of FITC-labeled R@T-NM solution to the hydrogel surface, intense green fluorescence was observed under 488 nm excitation (Figure 2C). Vertical sectioning of the hydrogel revealed extensive fluorescent signals throughout the matrix when examined by inverted fluorescence microscopy, confirming the penetration capability of R@T-NM (Figure 2D).

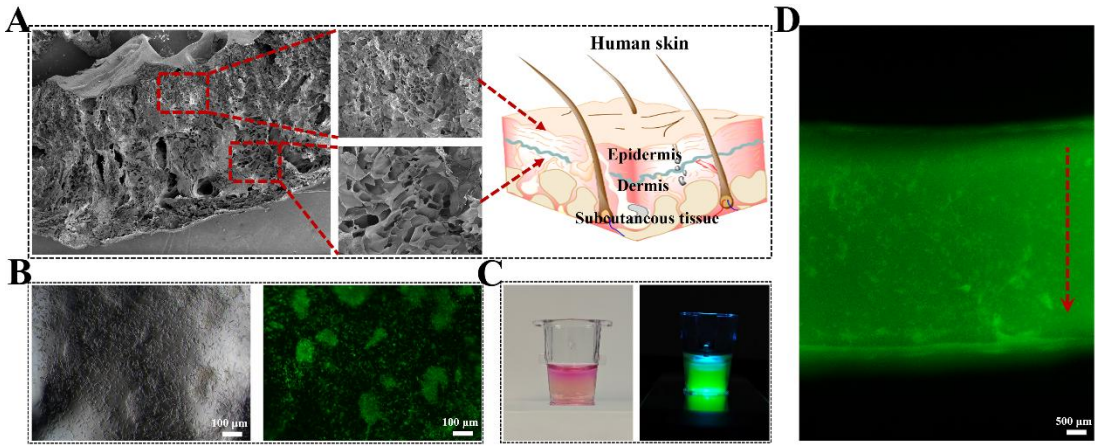

Figure 2. A) 3D Cellular Skin Models of GelMA hydrogel. B) Cells growth on GelMA hydrogels. C) Images of FITC-labeled R@T-NM after dropwise addition to the upper surface of a hydrogel. D) Images of FITC-labeled R@T-NM distribution within hydrogel.

3.3. Biocompatibility of R@T-NM

Using HSF cells as a model, cytotoxicity studies were conducted on R@T-NM, and the results are shown in **Figure 3**. The cytotoxicity of R@T-NM was evaluated over a concentration range of 5–30 μg/mL. It was found that the cell viability was ≥100% at concentrations below 10 μg/mL, indicating that low concentrations of R@T-NM promote the proliferation of HSF cells. When the concentration of R@T-NM was 15 μg/mL, the cell viability remained above 90%. Subsequently, Live/Dead cell staining was performed on all groups treated with 10 μg/mL R@T-NM solution. The results showed that the cells in each group exhibited intact morphology, with a spindle-shaped elongated appearance and minimal cell death. This demonstrates that even the R@T-NM system containing an organic solvent as a solubilizer also exhibits good biocompatibility.

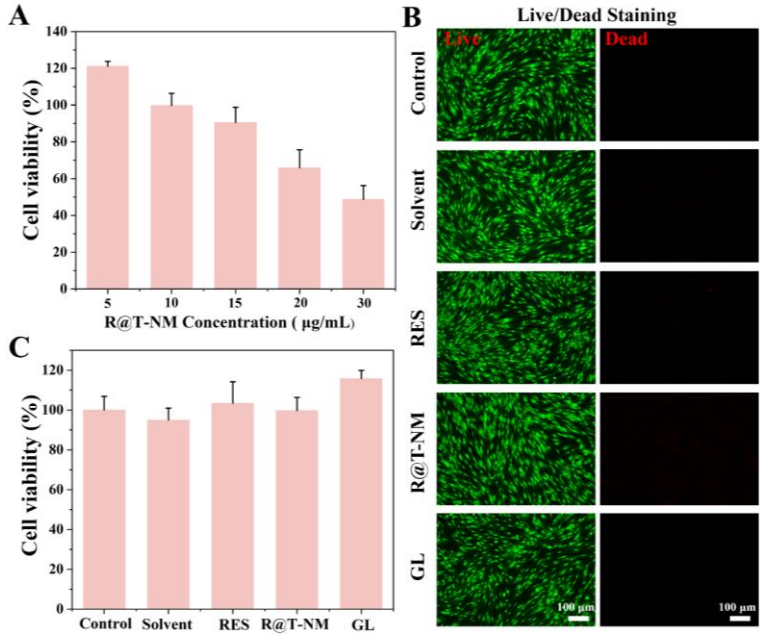

Figure 3. *In vitro* cytocompatibility of R@T-NM. A) Cytotoxicity of different concentrations of R@T-NM. B) Cytotoxicity and C) representative Live/Dead images of Solvent, RES, R@T-NM and GL groups treated with 10 μg/mL concentration. **p* < 0.05, ***p* < 0.01, ****p* < 0.001.

3.4. Antioxidant Capacity of R@T-NM

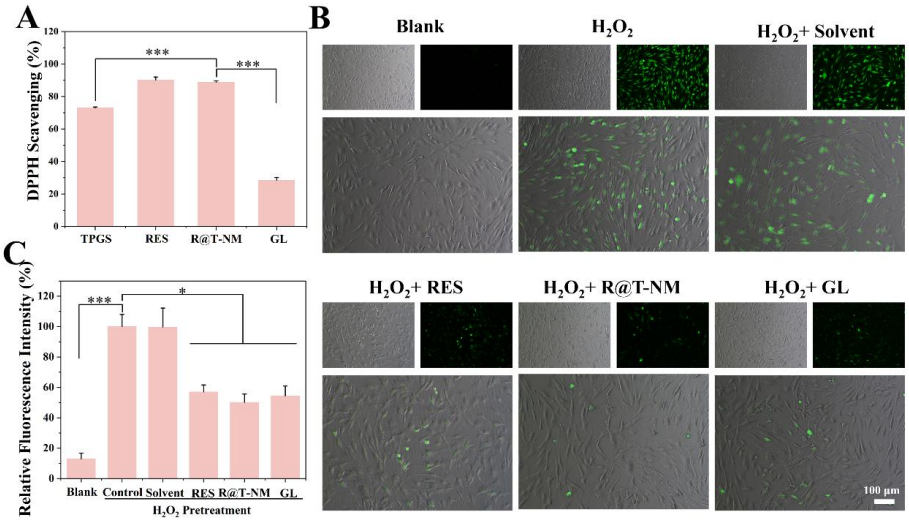

Figure 4. Antioxidant Capacity of R@T-NM. A) DPPH scavenging percentages of R@T-NM. B) the fluorescence images and C) relative fluorescence intensities of oxidation inhibition obtained by ROS test kit. **p* < 0.05, ***p* < 0.01, ****p* < 0.001.

The antioxidant activity of R@T-NM was evaluated by measuring its scavenging effect on DPPH radicals. As shown in **Figure 4A**, TPGS, RES, and R@T-NM all demonstrated strong DPPH radical scavenging capacities, with DPPH scavenging rates of 72.97%, 90.09%, and 88%, respectively, indicating superior antioxidant capability of TPGS, RES and R@T-NM. Elevated intracellular ROS levels can compromise cellular viability and potentially induce cell damage or apoptosis [20]. Using intracellular ROS scavenging assay to examine the ROS-scavenging capacity of R@T-NM in cells. **Figure 4B** reveals minimal green fluorescence signals in untreated control groups, confirming low basal ROS levels and healthy cellular status without apoptotic tendency. In contrast, treatment with 50 μM H_2O_2 markedly increased fluorescence intensity. However, co-treatment with RES, R@T-NM, or GL significantly attenuated this fluorescence signal. It is noteworthy that R@T-NM exhibited the weakest fluorescence

intensity among all treatment groups, yet it did not achieve the optimal free radical scavenging efficiency in the DPPH assay. This observation suggests that the antioxidant effect of RES may be rapidly depleted due to overreaction (e.g., rapid binding with free radicals). In contrast, TPGS likely prolongs RES's half-life by reducing its reactivity, thereby achieving a "sustained-release" effect. This further validates the protective role of TPGS in preserving RES activity.

3.5. Anti-inflammatory Activity of R@T-NM

To investigate the anti-inflammatary effect of R@T-NM, the expression levels of inflammation-related cytokines including IL-6 and IL-8 in HSF cells was determined using ELISA. As shown in **Figures 5A and 5B**, compared with the blank control group, LPS-stimulated HSF cells exhibited significantly elevated secretion of pro-inflammatory cytokines IL-6 and IL-8, indicating a successful stimulation of the cellular inflammatory state. However, treatment with R@T-NM markedly reduced the expression levels of both cytokines. These results demonstrate that R@T-NM can attenuate inflammatory responses by downregulating the expression of pro-inflammatory factors.

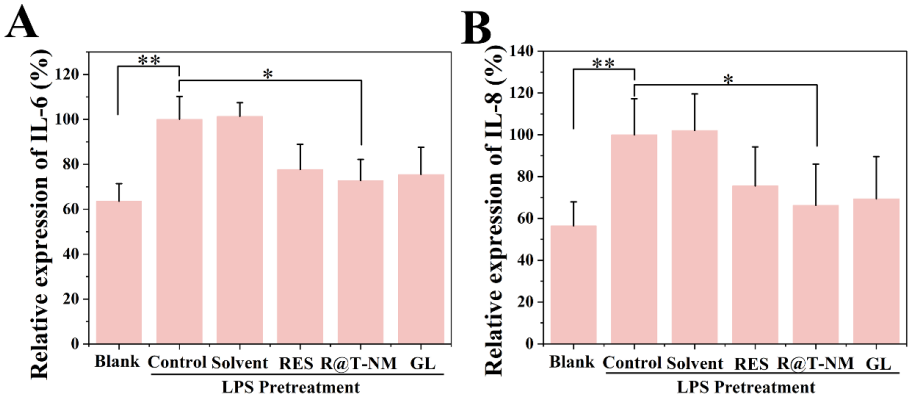

Figure 5. the relative expression levels of A) IL-6 and B) IL-8. *p < 0.05, **p < 0.01.

3.6. Anti-melanogenic Activity of R@T-NM

Skin complexion is closely related to the melanin produced by melanocytes in the basal layer of the epidermis. Tyrosinase, the rate-limiting enzyme in melanogenesis, serves as a key molecular target for skin whitening agents through its activity inhibition (**Figure 6A**) [21]. As demonstrated in **Figure 6B**, intracellular tyrosinase activity assays revealed that RES, R@T-NM, and GL exhibited significantly stronger tyrosinase inhibition compared to the control group. Notably, the R@T-NM treatment group showed the lowest tyrosinase activity levels, indicating its potent inhibitory effect on this pivotal enzyme and consequent skin-lightening potential.

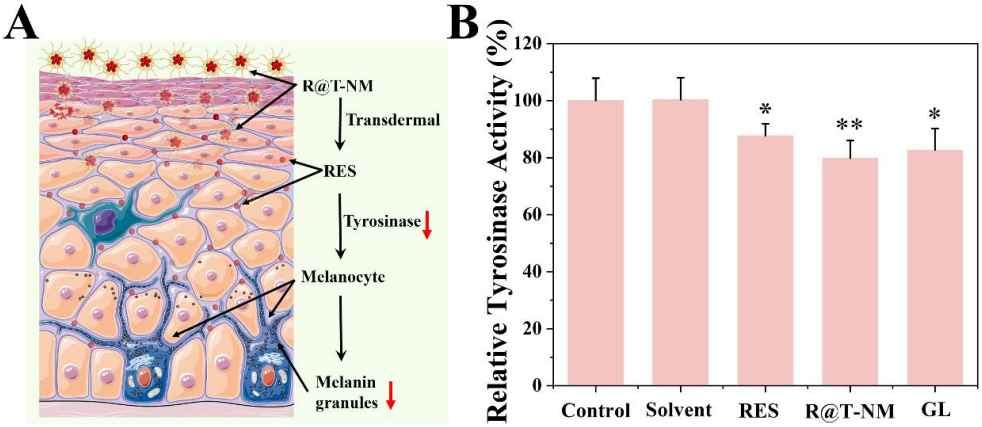

Figure 6. A) Schematic representation of the anti-melanogenic activity of R@T-NM. B) the relative expression levels of Tyrosinase. *p < 0.05, **p < 0.01, ***p < 0.001.

3.7 Evaluation of R@T-NM Anti-photoaging Effects

Cellular senescence, a hallmark of organismal aging, represents a state of permanent growth arrest in non-dividing cells. Based on literature review, we established a photoaging model by exposing HSF to UVA irradiation at an intensity of 5 J/cm² [22]. As shown in **Figure 7A**, five consecutive days of 5 J/cm² UVA exposure significantly increased the population of SA-β-galactosidase (SA-β-gal)-positive HSF cells. Comparative analysis revealed that UVA-irradiated HSF exhibited markedly higher SA-β-gal staining intensity versus the blank control group. Notably, treatment with resveratrol (RES), R@T-NM, or GL effectively counteracted UVA-induced cellular senescence. Among them, R@T-NM demonstrated the lowest percentage of SA-β-GAL-positive cells (**Figure 7B**), indicating its superior anti-photoaging activity, which was even better than that of glabridin (GL), a well-known whitening ingredient used by various famous cosmetic brands such as “Grain Rain”.

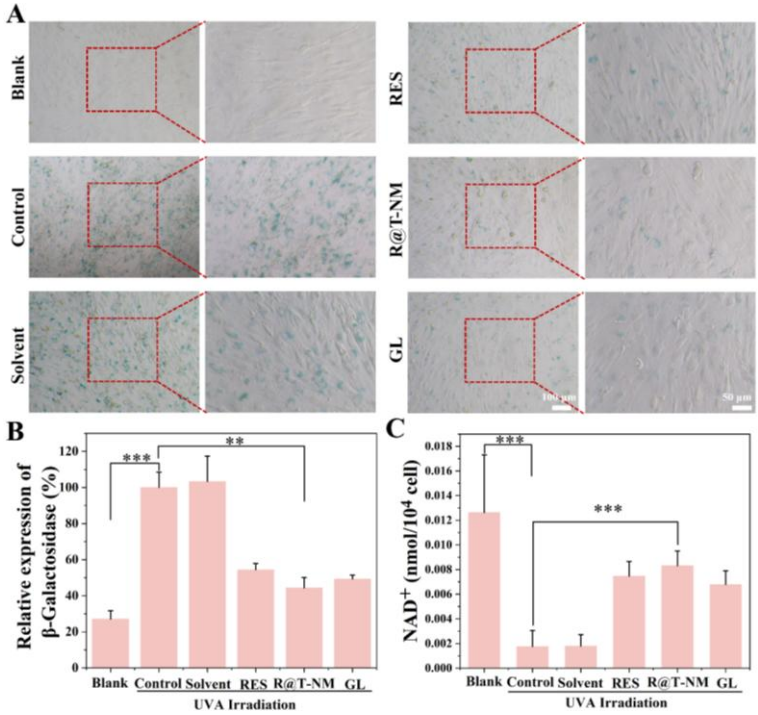

Figure 7. A) SA-β-gal staining of HSF cells and B) the relative expression levels of β-galactosidase. C) the expression levels of NAD^+. *p < 0.05, **p < 0.01, ***p < 0.001.

NAD^+ is ubiquitously present in eukaryotic cells. Research on aging based on metabolomics has demonstrated that NAD^+ serves as a crucial mediator in multiple key metabolic pathways, which are closely associated with cellular senescence. NAD^+ can inhibit oxidative stress, repair nuclear DNA damage, and modulate mitochondrial dysfunction, thereby impeding the process of cellular senescence [23]. In this study, we investigated the effects of R@T-NM on UVA-induced cellular senescence by measuring intracellular NAD^+ levels (**Figure 7C**). Compared with the blank control group, the NAD^+ content in HSF cells of the UVA group significantly decreased. However, compared with the UVA group, the NAD^+ content was significantly increased in the RES, R@T-NM, and GL treatment groups. These results indicate that R@T-NM can enhance NAD^+ expression and thus has potential in inhibiting cellular senescence.

4. Discussion

Resveratrol (RES) possesses a variety of pharmacological activities, including anti-inflammatory, antioxidant, anti-aging, anticancer, antitumor, blood glucose regulation, cardiocerebrovascular protection, cholesterol modulation, and antipyretic analgesic effects [24]. In the cosmetics industry, it primarily helps combat free radicals, delay skin aging, and brighten skin tone. However, RES has a low solubility of only 0.05 mg/mL in water, leading to a low bioavailability

in vivo [25]. Additionally, its structure contains multiple phenolic hydroxyl groups that are prone to photodegradation. Currently, microencapsulation/ nanoencapsulation techniques are commonly employed to encapsulate resveratrol within a phospholipid bilayer (e.g., liposomes) or polymer nanoparticles, thereby isolating it from the external environment and enhancing its stability and transdermal absorption rate [12]. In this study, the R@T-NM formulation, which encapsulates RES with TPGS, effectively improves the bioavailability, stability, and transdermal efficacy of RES, in addition to achieving protection of RES. TPGS, a water-soluble derivative of vitamin E, can synergistically enhance the multiple effects of RES.

Human aging is a complex biological process influenced by multiple factors, including genetics, environment, and metabolism. Long-term exposure of the skin to ultraviolet (UV) irradiation can accelerate skin aging. Oxidative stress is considered one of the key factors that contribute to accelerated aging [26]. R@T-NM, composed of the potent polyphenolic antioxidant resveratrol (RES) and the water-soluble vitamin E derivative tocopheryl polyethylene glycol succinate (TPGS), can provide electrons to neutralize reactive oxygen species (ROS) and effectively scavenge preformed free radicals. Literature has also shown that RES can inhibit the generation of free radicals at the source by upregulating the activity of endogenous antioxidant enzymes such as superoxide dismutase (SOD) and catalase (CAT) [27]. More notably, oxidative stress can activate key pro-inflammatory signaling pathways such as NF-κB. R@T-NM can significantly reduce the expression of pro-inflammatory factors, thereby breaking the vicious cycle of "oxidative stress-chronic inflammation" and slowing down the process of "inflammaging" at the molecular level.

R@T-NM can enhance the expression of NAD^+, which influences many key cellular functions, including metabolic pathways, DNA repair, chromatin remodeling, cellular senescence, and immune cell function [28]. This multifaceted enhancement allows R@T-NM to exert anti-aging effects on the skin through multiple mechanisms and at various levels. Tyrosinase, a key rate-limiting enzyme in melanin synthesis, can be overactivated by UV radiation, leading to UV-induced pigmentation (such as freckles and melasma), thereby exacerbating the signs of photoaging. Moreover, the large amounts of reactive oxygen species (ROS) generated by UV irradiation can directly activate tyrosinase and trigger the release of inflammatory factors (such as prostaglandin E_2, PGE_2), which further stimulate melanin synthesis [29]. R@T-NM can reduce the activity of tyrosinase and indirectly regulate its activity through its ROS-scavenging properties, thereby providing multidimensional photoprotective effects.

As an excellent ingredient with antioxidant, anti-inflammatory, and anti-aging properties, R@T-NM holds broad application prospects and development potential in the field of cosmetics.

5. Conclusion

In summary, R@T-NMs with sizes beneath 20 nm were developed for the first time. The ultrasmall size ensures favorable transdermal delivery, while the amphiphilic structure and inherent antioxidant properties of tocofersolan provide both spatial and molecular protection for resveratrol, reinforcing the potential of R@T-NM as a new generation anti-photoaging formulation. In the future, we plan to develop a series of anti-photoaging and anti-wrinkle formulations based on resveratrol and tocofersolan or other functional nanocarries.

Conflict of Interest Statement.

NONE.

References

[1] F Bernerd, T Passeron, I Castiel, C Marionnet (2022), The damaging effects of long UVA (UVA1) rays: A major challenge to preserve skin health and integrity, *Int. J. Mol. Sci.* 23(15):8243.
[2] X Tang, T Yang, D Yu, H Xiong, S Zhang (2024), Current insights and future perspectives of ultraviolet radiation (UV) exposure: Friends and foes to the skin and beyond the skin, *Environ. Int.* 185 108535.
[3] A Salminen, K Kaarniranta, A Kauppinen (2022), Photoaging: UV radiation-induced inflammation and immunosuppression accelerate the aging process in the skin, *Inflamm. Res.* 71(7) 817-831.
[4] P Alves, V Nieri, F Moreli, E Constantino, J-de Souza, Y Oshima-Franco, D Grotto (2024), Unveiling new horizons: Advancing technologies in cosmeceuticals for anti-aging solutions, *Molecules* 29(20):4890.
[5] M Calvo, C Navarro, P Durán, N Galan-Freyle, L Parra Hernández, L Pacheco-Londoño, D Castelanich, V Bermúdez, M Chacin (2024), Antioxidants in photoaging: From molecular insights to clinical applications, *Int. J. Mol. Sci*. 25(4):2403.
[6] X Yu, Y Jia, F Ren (2024), Multidimensional biological activities of resveratrol and its prospects and challenges in the health field, *Front. Nutr.* 11:1408651.
[7] H Liu, M Cheng, M Xun, Z Zhao, Y Zhang, W Tang, J Cheng, J Ni, W Wang (2023). Possible mechanisms of oxidative stress-induced skin cellular senescence, inflammation, and cancer and the therapeutic potential of plant polyphenols. *Int J Mol Sci*. 24(4):3755.
[8] S-A-O Shahcheraghi, F Salemi, S Small, S Syed, F Salari, W-A-O Alam, W-S Cheang, L Saso, HA-O Khan, Resveratrol regulates inflammation and improves oxidative stress via Nrf2 signaling pathway: Therapeutic and biotechnological prospects, *Phytother. Res.* 37(4):1590-1605.
[9] S Sheweita, Y El-Masry, T Zaghloul, S Mostafa, N Elgindy (2022), Preclinical studies on melanogenesis proteins using a resveratrol-nanoformula as a skin whitener, *Int. J. Biol. Macromol.* 223:870-881.
[10] T Meng, D Xiao, A Muhammed, J Deng, L Chen, J He (2021), Anti-Inflammatory action and mechanisms of resveratrol, *Molecules*, 26(1):229.
[11] A Santos, I Pereira, M Pereira-Silva, L Ferreira, M Caldas, M Collado-González, M Magalhães, A Figueiras, A J Ribeiro, F Veiga (2019), Nanotechnology-based formulations for resveratrol delivery: Effects on resveratrol in vivo bioavailability and bioactivity, *Colloids Surf B* 180:127-140.
[12] Y Song, J Zhang, L Zhu, H Zhang, G Wu, T Liu (2024), Recent advances in nanodelivery systems of resveratrol and their biomedical and food applications: a review, *Food funct.* 15(17) 8629-8643.
[13] A Mehandole, N Walke, S Mahajan, M Aalhate, I Maji, U Gupta, N K Mehra, P K Singh (2023), Core-shell type lipidic and polymeric nanocapsules: the transformative multifaceted delivery systems, *AAPS Pharm Sci Tech* 24(1):50.
[14] D Patel, K Kuperkar, S-i Yusa, P Bahadur (2023), Nanoscale self-assemblies from amphiphilic block copolymers as proficient templates in drug delivery, *Drugs Drug Candidates*, 2(4):898-922.
[15] Y Guo, J Luo, S Tan, B O Otieno, Z Zhang (2013), The applications of Vitamin E TPGS in drug delivery, *Eur J Pharm Sci,* 49(2):175-86.
[16] G Zuccari, S Alfei, A Zorzoli, D Marimpietri, F Turrini, S Baldassari, L Marchitto, G Caviglioli (2021), Increased water-solubility and maintained antioxidant power of resveratrol by its encapsulation in vitamin E TPGS micelles: A potential nutritional supplement for chronic liver disease, *Pharmaceutics* 13(8):1128.
[17] C Yang, T Wu, Y Qi, Z Zhang (2018), Recent advances in the application of vitamin E TPGS for drug delivery, *Theranostics* 8(2):464-485.
[18] D Liu, S Qiao, B Cheng, D Li, J Chen, Q Wu, H Pan, W Pan (2020), Enhanced oral delivery of curcumin via vitamin E TPGS modified nanodiamonds: a comparative study on the efficacy of non-covalent and covalent conjugated strategies, *AAPS Pharm Sci Tech* 21(5):187.
[19] S Supe, P Takudage (2021), Methods for evaluating penetration of drug into the skin: A review, *Skin Res Technol,* 27(3):299-308.
[20] D Zhou, M Luo, S Huang, A Saimaiti, A Shang, R Gan, H Li (2021), Effects and mechanisms of resveratrol on aging and age-related diseases, oxidative medicine and cellular longevity, *Oxid Med Cell Longev,* 2021:9932218.
[21] T Pillaiyar, M Manickam, V Namasivayam (2017), Skin whitening agents: medicinal chemistry perspective of tyrosinase inhibitors, *J. Enzyme Inhib Med Chem* 32(1):403-425.
[22] G Bai, P Wang, X Huang, Z Wang, D Cao, C Liu, Y Liu, R Li, A Chen (2021), Rapamycin protects skin fibroblasts from UVA-induced photoaging by inhibition of p53 and phosphorylated HSP27, *Front Cell Dev Biol,* 9:633331
[23] C Chini, H Cordeiro, N Tran, E Chini (2024), NAD metabolism: Role in senescence regulation and aging, *Aging Cell* 23(1):e13920.

[24] A Kaur, R Tiwari, G Tiwari, V Ramachandran (2022), Resveratrol: A vital therapeutic agent with multiple health benefits, *Drug research,* 72(1):5-17.
[25] J Gambini, M Inglés, G Olaso, R Lopez-Grueso, V Bonet-Costa, L Gimeno-Mallench, C Mas-Bargues, K Abdelaziz, M Gomez-Cabrera, J Vina, C Borras (2015), Properties of resveratrol: In vitro and in vivo studies about metabolism, bioavailability, and biological effects in animal models and humans, *Oxid Med Cell Longev,* 2015:837042.
[26] U Panich, G Sittithumcharee, N Rathviboon, S Jirawatnotai (2016), Ultraviolet radiation-induced skin aging: The role of DNA damage and oxidative stress in epidermal stem cell damage mediated skin aging, *Stem Cells Int,* 2016:7370642.
[27] M Mokni, S Elkahoui, F Limam, M Amri, E Aouani (2007), Effect of resveratrol on antioxidant enzyme activities in the brain of healthy rat, *Neurochem Res,* 32(6):981-7.
[28] A Covarrubias, R Perrone, A Grozio, E Verdin (2021), NAD(+) metabolism and its roles in cellular processes during ageing, *Nat Rev Mol Cell Biol,* 22(2):119-141.
[29] S Pillai, C Oresajo, J Hayward (2005), Ultraviolet radiation and skin aging: roles of reactive oxygen species, inflammation and protease activation, and strategies for prevention of inflammation-induced matrix degradation - a review, *Int J Cosmet Sci*, 27(1):17-34.